Naval Research Laboratory

Washington, DC 20375-5000

NRL Memorandum Report 6620

Foil Focusing of Electron Beams

R. F. FERNSLER, R. F. HUBBARD AND S. P. SLINKER

Beam Physics Branch
Plasma Physics Division

March 14, 1990

Approved for public release; distribution unlimited.

REPORT DOCUMENTATION PAGE

Form Approved
OMB No. 0704-0188

1. AGENCY USE ONLY (Leave blank)	2. REPORT DATE	3. REPORT TYPE AND DATES COVERED
	1990 March 14	Interim

4. TITLE AND SUBTITLE

Foil Focusing of Electron Beams

5. FUNDING NUMBERS

47-0900-0-0 (JO#)
ARPA Order #4395, A86

6. AUTHOR(S)

Fernsler, R. F., Hubbard, R. F., and Slinker, S. P.

7. PERFORMING ORGANIZATION NAME(S) AND ADDRESS(ES)

Naval Research Laboratory
Washington, DC 20375-5000

8. PERFORMING ORGANIZATION REPORT NUMBER

9. SPONSORING/MONITORING AGENCY NAME(S) AND ADDRESS(ES)

DARPA
Arlington, VA 22209

NSWC
Silver Spring, MD 20903-5000

10. SPONSORING/MONITORING AGENCY REPORT NUMBER

11. SUPPLEMENTARY NOTES

12a. DISTRIBUTION/AVAILABILITY STATEMENT

Approved for public release; distribution unlimited.

12b. DISTRIBUTION CODE

13. ABSTRACT *(Maximum 200 words)*

Thin conducting foils focus charged particle beams through image charges induced on the foils. Such focusing has led to the suggestion that foils be used to transport intense, relativistic electron beams in high-energy accelerators. This paper examines some of the limitations of foil focusing including sensitivity to the beam parameters, emittance growth from anharmonic focusing, and beam stability in multi-foil transport. The analysis is based on a thin-lens, electrostatic treatment of paraxial beams.

14. SUBJECT TERMS

Foils materials;
Electron beams focusing;
Linear Accelerators. (EDC)

15. NUMBER OF PAGES

16. PRICE CODE

17. SECURITY CLASSIFICATION OF REPORT	18. SECURITY CLASSIFICATION OF THIS PAGE	19. SECURITY CLASSIFICATION OF ABSTRACT	20. LIMITATION OF ABSTRACT
UNCLASSIFIED	UNCLASSIFIED	UNCLASSIFIED	SAR

NSN 7540-01-280-5500

Standard Form 298 (Rev 2-89)
Prescribed by ANSI Std Z39-18
298-102

CONTENTS

FOIL FOCUSING OF ELECTRON BEAMS

I. INTRODUCTION

Accelerating intense, high-current electron beams to ultrarelativistic energies requires a focusing mechanism to overcome the defocusing from beam emittance and space-charge. The need for focusing is most critical in the initial accelerator stages when the beam energy γ is smallest. As γ rises, the need for focusing decreases because the azimuthal magnetic field of the beam offsets the defocusing space-charge field to order γ^{-2}, and because the unnormalized beam emittance decreases as γ^{-1} in an ideal accelerator.[1]

The two main focusing methods used in high-current linear induction accelerators are solenoidal fields and, more recently, radial electrostatic fields from an ion column.[2] Solenoidal focusing requires precise magnetic alignment and a large investment in magnetic energy. Ion focusing, on the other hand, requires a plasma column with the attendant problems of gas pumping, plasma instabilities, loading of the accelerating gaps, etc. Both transport techniques are, moreover, subject to beam instabilities, either from cavity modes[3] or from ion motion.[4]

An alternative transport technique, first suggested by Adler,[5] is a series of thin conducting foils placed transverse to the beam axis. Foils act like thin electrostatic lenses that focus the beam via image charges. Foils are easy to implement and may help stabilize the beam.[5,6] Initial experimental studies[6-8] of foil focusing were encouraging, although Meger[9] has reported difficulty at beam currents above 10 kA.

In this paper we model foil focusing using the thin-lens approximation assumed by Adler[5] and Humphries.[10] With this model we determine the dependence of foil focusing on the beam parameters, study its effect on beam emittance, and examine stability of multi-foil transport. Although the thin-lens approximation is generally valid only for paraxial beams of current $I_b \ll 17\gamma$ kA, preliminary numerical simulations suggest that the analytical predictions remain roughly intact even when the paraxial approximation fails. The numerical simulations will be presented in a later publication.

Manuscript approved January 30, 1990.

The paper is organized as follows. The focusing properties of an isolated thin foil are determined in Sec. II for several different, axisymmetric beam profiles. Emittance growth from anharmonic foil focusing is computed in Sec. III. Multi-foil transport, including beam stability and electrical interactions between adjacent foils, is considered in Sec. IV. Apertures, foil scattering, plasma effects, and beam centering are covered briefly in Sec. V. Section VI summarizes the results.

II. FOIL FOCUSING

A. Electrostatic Potential from a Single, Thin Foil

A conducting foil placed perpendicular to the path of an electron beam induces foil currents and charges that short the electromagnetic fields of the beam. The foil charges produce electrostatic fields that persist well outside the foil and act to focus the beam. The foil currents, on the other hand, little affect the beam because they are closely spaced and flow anti-parallel on the two faces of the foil. The primary effect of the foil, therefore, is to focus the beam electrostatically.[11] In this section we compute the electrostatic foil fields for several different beam profiles.

To model foil focusing, consider an ultrarelativistic, paraxial beam propagating in a conducting pipe of radius b. The beam is paraxial in that the beam electrons follow nearly straight and parallel orbits over axial distances ~ b. This assumption allows us to treat the foil as a thin but imperfect lens. In addition, we neglect foil scattering and assume that neither the beam current nor radius changes rapidly within a time b/c. The last assumption allows us to neglect inductive and time-retardation corrections to the fields.

The foil charge produces an electrostatic potential satisfying

$$\nabla^2 \phi_f = 0, \tag{1}$$

with ϕ_f equal to zero at $z = \pm\infty$ and on the pipe, $r = b$. On the foil itself,

$$\phi_f = - \phi_o, \tag{2}$$

where ϕ_o is the potential from the beam (and associated plasma, if any) in the absence of the foil. The foil thus converts the ambient transverse field, $\underset{\sim}{E}_{\perp o} = -\underset{\sim}{\nabla}_\perp \phi_o$, into a longitudinal field, $E_{zf} = -\partial\phi_f/\partial z$. The longitudinal foil field E_{zf} accelerates the beam as it approaches the foil and decelerates the beam as it leaves the foil. The major influence on beam dynamics, however, is the electrostatic pinch caused by $\underset{\sim}{\nabla}_\perp \phi_f$. The longitudinal field E_{zf} is much less important because it is anti-symmetric about the foil, and because the transverse energy of a paraxial beam is much smaller than the longitudinal energy.

For an axisymmetric beam, a single foil located at $z = 0$ generates an electrostatic potential that can be expressed as

$$\phi_f(r,z) = \sum_{n=1}^{\infty} A_n \exp(-\chi_n |z|/b)\, J_o(\chi_n r/b), \tag{3}$$

where χ_n is the nth root of the Bessel function J_o and

$$A_n = -\frac{2}{b^2 J_1^2(\chi_n)} \int_0^b dr\, r\, J_o(\chi_n r/b)\, \phi_o(r,0) \tag{4a}$$

$$= -\frac{2}{\chi_n b\, J_1^2(\chi_n)} \int_0^b dr\, r\, J_1(\chi_n r/b)\, E_{ro}(r,0) \tag{4b}$$

$$= -\frac{2}{\chi_n^2 J_1^2(\chi_n)} \int_0^b dr\, r\, J_o(\chi_n r/b) \left[\frac{1}{r}\frac{\partial}{\partial r}\, r\, E_{ro}(r,0)\right]. \tag{4c}$$

Here $E_{ro} = -\partial\phi_o/\partial r$ is the radial electrostatic field from the beam and plasma, and we have integrated by parts using the Bessel identities, $J_1(x) = -\,dJ_o/dx$ and $xJ_o(x) = d(xJ_1)/dx$.

B. Radial Impulse Produced by a Foil

As Eq. (3) demonstrates, the foil pinch field, $E_{rf} = -\partial\phi_f/\partial r$, is strong only within an axial distance $\sim b/\chi_1$. In this short distance, the foil alters the radial momentum but not the orbital radius of the paraxial electrons. Assuming no change in radius r or axial velocity v_z, the electrons acquire a radial impulse given by

$$\delta p_r(r) = -\int_{-\infty}^{\infty} dz\, \frac{e}{v_z} \frac{\partial \phi_f}{\partial r} = \frac{2e}{c} \sum_{n=1}^{\infty} A_n\, J_1(\chi_n r/b). \tag{5}$$

Here we have set v_z equal to the speed of light, c. The assumption of constant r and constant v_z constitutes the thin-lens approximation.

To quantify the analysis, consider a rigid-rod beam and a plasma that neutralizes the beam charge by a fraction $f_c(r) \leq 1$. Most applications operate in vacuum where $f_c = 0$, but for generality we allow $f_c \neq 0$. For a long rigid-rod beam, $\partial/\partial z = 0$ and the ambient space-charge field from the beam and plasma satisfies

$$\frac{1}{r} \frac{\partial}{\partial r}\, r\, E_{ro} = \frac{4\pi}{c} (1-f_c) J_b, \tag{6}$$

where $J_b(r)$ is the beam current density. Inserting Eq. (6) into Eq. (4c) yields

$$A_n = -\left(\frac{2}{\chi_n J_1(\chi_n)}\right)^2 \frac{2\pi}{c} \int_0^b dr\, r\, (1-f_c) J_b(r,0)\, J_o(\chi_n r/b). \tag{7}$$

We now compute A_n for four different beam profiles, assuming constant f_c. The influence of the foil on f_c is discussed later.

For a flat-topped beam with J_b constant out to a radius $r_b < b$, Eq. (7) reduces to

$$A_n = -\,8\, \frac{(1-f_c) I_b}{c}\, \frac{b}{r_b}\, \frac{J_1(\chi_n r_b/b)}{\chi_n^3\, J_1^2(\chi_n)}, \tag{8a}$$

where $I_b = \pi r_b^2 J_b$ is the beam current. Inserting Eq. (8a) into the impulse equation (5) yields Adler's[5] result for the deflection angle from the foil:

$$\delta\theta_f = \frac{\delta p_r}{p_z} = -\,16\, \frac{(1-f_c) I_b}{I_A}\, \frac{b}{r_b} \sum_{n=1}^{\infty} \frac{J_1(\chi_n r_b/b)\, J_1(\chi_n r/b)}{\chi_n^3\, J_1^2(\chi_n)}, \tag{8b}$$

where $p_z = \gamma mc$ is the axial momentum, $I_A = \gamma mc^3/e \simeq 17\gamma$ kA is the Alfven current, and γ is the Lorentz factor. The mean-squared radius for a flat-topped beam is $R^2 = r_b^2/2$.

For a Gaussian beam with J_b varying as $\exp(-r^2/R^2)$,

$$A_n = - \left(\frac{2}{\chi_n J_1(\chi_n)}\right)^2 \frac{(1-f_c)I_b}{c} \exp[-(\chi_n R/2b)^2], \tag{9a}$$

and

$$\delta\theta_f = - 8 \frac{(1-f_c)I_b}{I_A} \sum_{n=1}^{\infty} \frac{\exp[-(\chi_n R/2b)^2]}{\chi_n^2 J_1^2(\chi_n)} J_1(\chi_n r/b), \tag{9b}$$

to order $\exp(-b^2/R^2)$. The rms radius equals R.

For a parabolic beam with J_b varying as $(1-r^2/r_b^2)$ for $r \leq r_b$,

$$A_n = - \frac{(1-f_c)I_b}{c} \left(\frac{8b/r_b}{\chi_n^2 J_1(\chi_n)}\right)^2 \left[\frac{b}{\chi_n r_b} J_1(\chi_n r_b/b) - \frac{J_o(\chi_n r_b/b)}{2}\right], \tag{10a}$$

and

$$\delta\theta_f = - \frac{(1-f_c)I_b}{I_A} \sum_{n=1}^{\infty} \left(\frac{8b/r_b}{\chi_n^2 J_1(\chi_n)}\right)^2 J_1(\chi_n r/b) \left[\frac{b}{\chi_n r_b} J_1(\chi_n r_b/b) - \frac{J_o(\chi_n r_b/b)}{2}\right]. \tag{10b}$$

The mean-squared radius is $R^2 = r_b^2/3$.

For a Bessel profile with J_b varying as $J_o(\chi_1 r/r_b)$ for $r \leq r_b$,

$$A_n = - 4 \frac{(1-f_c)I_b}{c} \left(\frac{\chi_1}{\chi_n}\right)^2 \frac{J_o(\chi_n r_b/b)}{J_1^2(\chi_n)\,[\chi_1^2 - (\chi_n r_b/b)^2]}, \tag{11a}$$

and

$$\delta\theta_f = - 8 \frac{(1-f_c)I_b}{I_A} \sum_{n=1}^{\infty} \left(\frac{\chi_1}{\chi_n}\right)^2 \frac{J_o(\chi_n r_b/b)\, J_1(\chi_n r/b)}{J_1^2(\chi_n)\,[\chi_1^2 - (\chi_n r_b/b)^2]}. \tag{11b}$$

The mean-squared radius is $R^2 = (1-4/\chi_1^2) r_b^2 \simeq (0.555\ r_b)^2$.

C. Foil Focal Length

In Fig. 1 we plot the foil focal length,

$$f_\ell(r) \equiv - r/\delta\theta_f(r), \tag{12}$$

for three values of b/R for each of the four profiles. For all profiles, f_ℓ is proportional to $\gamma R/(1-f_c)I_b$, and it increases with particle radius r but decreases with wall radius b. The dependence on r means that the lens is imperfect, with the beam image distorted and emittance degraded. Any spread in particle energy in a given transverse segment of the beam further degrades the emittance through the dependence of f_ℓ on γ. The variation in f_ℓ with r is the least for a flat-topped beam, for which the self-field E_{ro} is harmonic (proportional to r for $r \leq r_b$), and is the greatest for the Gaussian profile which extends to large r. The parabolic and Bessel profiles both cut off sharply and produce nearly identical f_ℓ.

The dependence of the focal length on the beam parameters makes foil focusing difficult to control, but it also provides a means for altering the beam envelope, $R(\zeta)$; here $\zeta = ct-z$ measures distance into the beam pulse. Controlled manipulation of $R(\zeta)$ is possible only in regions where I_b/γ varies in a known manner with ζ. Unpredictable fluctuations in I_b, γ, or R produce like fluctuations in f_ℓ that can grow with propagation distance z. See Sec. IV for further discussion.

The paraxial approximation is valid only if $f_\ell \gg b$, or equivalently, $\delta\theta_f \ll 1$. For foils, this requires that $(1-f_c)I_b \ll I_A$. At high beam currents, $I_b \gtrsim 0.3\ I_A/(1-f_c)$, foil focusing becomes so strong that the axial and transverse particle velocities become comparable. Beam quality is then poor, although efficient foil transport is possible even at currents above the space-charge limiting current.[6]

III. BRAM EMITTANCE

A. Imperfect Lenses

A useful parameter for characterizing beam quality is the rms transverse emittance. For simplicity, we consider an axisymmetric. non-rotating, monoenergetic beam with a normalized emittance defined by[12]

$$\varepsilon = \gamma\ [R^2\langle\beta_\perp{}^2\rangle - \langle\underset{\sim}{r}_\perp\cdot\underset{\sim}{\beta}_\perp\rangle^2]^{1/2}, \tag{13}$$

where the mean-squared beam radius is given by

$$R^2 = \langle \underset{\sim}{r}_\perp{}^2 \rangle, \tag{14}$$

and $\underset{\sim}{r}_\perp$ and $\underset{\sim}{\beta}_\perp = d\underset{\sim}{r}_\perp/dz$ are the transverse position and velocity, respectively, of a beam electron. The angular brackets denote an average taken over all particles in a given transverse segment. Harmonic forces preserve ε, but anharmonic forces generally do not.[1] In an ideal accelerator with harmonic forces, the unnormalized emittance ε/γ determines beam expansion and decreases as γ rises.

To compute the emittance change produced by an anharmonic thin lens, we express the transverse velocity of each beam electron as

$$\underset{\sim}{\beta}_\perp = \beta_r \hat{r} + \delta\underset{\sim}{\beta}_\perp, \tag{15}$$

where $\delta\underset{\sim}{\beta}_\perp$ is a random thermal velocity and β_r is the radial fluid velocity defined by

$$\beta_r(r,\zeta) = \iint d^2\underset{\sim}{\beta}_\perp \; \underset{\sim}{\beta}_\perp \cdot \hat{r} \;\; F(\underset{\sim}{r}_\perp, \underset{\sim}{\beta}_\perp, \zeta). \tag{16}$$

Here $F(\underset{\sim}{r}_\perp, \underset{\sim}{\beta}_\perp, \zeta)$ is the electron distribution function, and $\hat{r}$ is the unit radial vector. The thermal component satisfies by definition

$$\iint d^2\underset{\sim}{\beta}_\perp \; \delta\underset{\sim}{\beta}_\perp \cdot \hat{r} \;\; F(\underset{\sim}{r}_\perp, \underset{\sim}{\beta}_\perp, \zeta) = 0. \tag{17}$$

A thin lens alters $\underset{\sim}{\beta}_\perp$ by $\delta\theta_f \hat{r}$:

$$\underset{\sim}{\beta}_\perp \rightarrow \underset{\sim}{\beta}_\perp + \delta\theta_f \hat{r} = \delta\underset{\sim}{\beta}_\perp + [\beta_r - (r/f_\ell)]\hat{r}. \tag{18}$$

According to Eqs. (13)-(17), this alters the square of the emittance by

$$\delta(\varepsilon^2) = \varepsilon_{fo}^2 + \varepsilon_{f1}^2, \tag{19}$$

where

$$\varepsilon_{fo}^2 \equiv \gamma^2 \left[R^2 \langle (r/f_\ell)^2 \rangle - \langle r^2/f_\ell \rangle^2\right], \tag{20a}$$

and

$$\varepsilon_{f1}^2 \equiv 2\gamma^2 \left[\langle r^2/f_\ell\rangle \langle\beta_r r\rangle - R^2 \langle\beta_r r/f_\ell\rangle\right]. \tag{20b}$$

The emittance change ε_{fo}^2 is independent of the beam velocity distribution and is always positive; by contrast, ε_{f1}^2 is controlled by changes in the beam profile and can be positive or negative. In deriving Eq. (19), we have used the fact that

$$\langle g(r)\ \delta\underset{\sim}{\beta}_\perp \cdot \hat{r}\rangle = 0, \tag{21}$$

for all $g(r)$.

Several points are worth noting from results (19) and (20). First, a perfect lens does not alter the beam emittance: $\varepsilon_{fo} = \varepsilon_{f1} = \delta\varepsilon = 0$ for $\partial f_\ell/\partial r = 0$. Second, the change in emittance from an imperfect lens is independent of the beam thermal velocity $\delta\underset{\sim}{\beta}_\perp$; a hot beam thus suffers the same emittance change as a cold beam, assuming identical fluid velocity $\beta_r(r,\zeta)$. Third, if the beam evolves self-similarly,[12] the term ε_{f1} equals zero and the emittance squared increases by $\varepsilon_{fo}^2 > 0$; self-similar evolution means that the beam profile is invariant, with $u_r \propto r/R$ and $J_b R^2$ a function of r/R only. An anharmonic thin lens thus increases the square of the emittance by ε_{fo}^2, unless the beam changes its profile while striking the lens. We defer discussion of profile changes until Sec. III-C.

B. Scaling of ε_{fo}

The emittance increase ε_{fo} can be estimated using a generic model for the foil focal length:

$$f_\ell(r) \simeq g_o R\, \frac{I_A}{(1-f_c)I_b}\,(1 + g_1 r^2/R^2), \tag{22a}$$

where g_o characterizes the lens strength and g_1 is an anharmonic lens coefficient. This form fits the four profiles in Fig. 1 well for $r \lesssim 2R$. Table 1 lists the approximate coefficients g_o and g_1 for the flat-topped, Gaussian, parabolic, and Bessel profiles for several values of b/R. The anharmonic coefficient g_1 is smallest for the flat-topped profile and largest for the Gaussian profile.

TABLE 1: VALUES OF (g_o, g_1)

Beam Profile	b/R = 2	5	10
Flat-topped	(0.45, 0.12)	(0.37, 0.13)	(0.35, 0.12)
Gaussian	(0.37, 0.42)	(0.31, 0.28)	(0.3, 0.24)
Parabolic	(0.38, 0.22)	(0.35, 0.15)	(0.32, 0.18)
Bessel	(0.38, 0.2)	(0.34, 0.19)	(0.32, 0.18)

Inserting approximation (22a) into emittance definition (20a) produces

$$\varepsilon_{fo} = \alpha \frac{(1-f_c)I_b}{mc^3/e} \simeq \alpha \frac{(1-f_c)I_b}{17\ kA} R, \tag{22b}$$

where α is a dimensionless coefficient that depends on the beam profile. For example, for a flat-topped profile,

$$\langle (r/f_\ell)^2 \rangle = \frac{1}{2} \left(\frac{(1-f_c)I_b}{g_o I_A} \right)^2 \int_0^2 dx \frac{x}{(1+g_1 x)^2}, \tag{23a}$$

and

$$\langle r^2/f_\ell \rangle = \frac{R}{2g_o} \frac{(1-f_c)I_b}{I_A} \int_0^2 dx \frac{x}{1+g_1 x}, \tag{23b}$$

where $x = r^2/R^2$. Performing the integrals and substituting the results into Eq. (20a) yields

$$\varepsilon_{fo} = \frac{R}{2^{1/2} g_o g_1} \frac{(1-f_c)I_b}{mc^3/e} \left[\frac{(1+2g_1)\ \ln(1+2g_1) - 2g_1}{1+2g_1} - 2 \left(\frac{2g_1 - \ln(1+2g_1)}{2g_1} \right)^2 \right]^{1/2}. \tag{23c}$$

Using the values for g_o and g_1 from Table 1, we compute the emittance coefficient for a flat-topped beam to be

$$\alpha \simeq 0.1, \tag{23d}$$

with a weak dependence on b/r_b.

Similarly, for the Gaussian profile,

$$\langle (r/f_\ell)^2 \rangle = \left(\frac{(1-f_c)I_b}{g_o I_A} \right)^2 \left(1-e^{-b^2/R^2} \right)^{-1} \int_0^{(b/R)^2} dx \frac{}{(1+g_1 x)^2} e^{-x}, \tag{24a}$$

and

$$\langle r^2/f_\ell \rangle = \frac{R}{g_o} \frac{(1-f_c)I_b}{I_A} \left(1 - e^{-b^2/R^2}\right)^{-1} \int_0^{(b/R)^2} dx \frac{x}{1+g_1 x} e^{-x}. \quad (24b)$$

For $b > 3R$, Eqs. (20a), (24a) and (24b) can be combined into

$$\varepsilon_{fo} \simeq \frac{R}{g_o g_1} \frac{(1-f_c)I_b}{mc^3/e} \left(g_1 - (1+g_1)\, y(g_1) - [y(g_1)]^2\right)^{1/2}, \quad (24c)$$

where

$$y(g) = e^{1/g} \int_1^\infty dt \frac{e^{-t/g}}{t^2}$$

can be expressed in terms of an exponential integral. Typically, the emittance coefficient for a Gaussian beam is given by

$$\alpha \simeq 0.5, \quad (24d)$$

five times larger than the flat-topped coefficient (23d).

For the parabolic profile,

$$\langle (r/f_\ell)^2 \rangle = \frac{2}{3} \left(\frac{(1-f_c)I_b}{g_o I_A}\right)^2 \int_0^3 dx \frac{x\,(1-x/3)}{(1+g_1 x)^2}, \quad (25a)$$

and

$$\langle r^2/f_\ell \rangle = \frac{2}{3} \frac{R}{g_o} \frac{(1-f_c)I_b}{I_A} \int_0^3 dx \frac{x(1-x/3)}{1+g_1 x}. \quad (25b)$$

Performing the integrals and substituting the results into Eq. (20a) yields

$$\varepsilon_{fo} = \left(\frac{2}{9}\right)^{1/2} \frac{R}{g_o g_1^{3/2}} \frac{(1-f_c)I_b}{mc^3/e} \left[(2+3g_1)\ln(1+3g_1) - 6g_1 - \frac{2}{9} g_1^{-3} \left(\frac{9}{2} g_1^2 + 3g_1 - (1+3g_1)\ln(1+3g_1)\right)^2\right]^{1/2}. \quad (25c)$$

A typical emittance coefficient for a parabolic profile is

$$\alpha \simeq 0.2, \tag{25d}$$

roughly half-way between the flat-topped and Gaussian coefficients. A Bessel profile should produce similar results.

C. Consequences of Emittance Growth

The preceding equations demonstrate that the emittance increase ε_{fo} from foil focusing scales linearly with beam current and radius, is independent of γ, and depends strongly on the beam profile. High-current beams with broad radial wings, such as Gaussian or Bennett profiles, suffer the largest increase. As Eqs. (23d) and (24d) illustrate, the presumption of a flat-topped profile can underestimate ε_{fo} by a factor of five or more.

The significance of ε_{fo} can be determined by comparing it with the emittance desired for the beam outside the accelerator. A paraxial beam propagates in equilibrium in a gas only if its emittance equals

$$\varepsilon_{eq} = \gamma R \, (I_{eff}/I_A)^{1/2}, \tag{26}$$

where $I_{eff} < I_b$ is an effective current that characterizes the pinch force felt by the beam. In a dense gas, I_{eff} equals the sum of the beam current and the inductively generated plasma-return current.[13] In a low-pressure gas, I_{eff} measures the strength of the plasma ion channel.[14]

The cumulative emittance gained by a beam after passing through n foils, each with an emittance increase of ε_{fo}, is less than ε_{eq} only if

$$n < \frac{I_{eff} I_A}{[\alpha(1-f_c)I_b]^2}, \tag{27}$$

assuming constant radius R. For $f_c = 0$ and $I_{eff} \sim I_b$, the number of foils is limited to $n < I_A/\alpha^2 I_b$, which depends strongly on beam profile through the parameter α. To increase the number of allowed foils, or to transport high-quality beams with $I_{eff} \ll I_b$, plasma must be added to produce $f_c > 0$. Adding plasma eliminates, however, the need for foil focusing. Emittance growth from anharmonic focusing thus limits the utility of foil transport, especially for high-current beams with broad radial wings.

The emittance increase ε_{fo} could, if desired, be used to alter the emittance envelope, $\varepsilon(\zeta)$, of an initially cold beam. For example, a beam of constant radius but rising current would suffer the greatest emittance increase in the beam body, regardless of variations in γ. Alternatively, $\varepsilon(\zeta)$ could be modified by varying the beam radius R before the beam strikes the foil.

We have thus far neglected changes in the beam profile at the foil. Such changes either increase or decrease the emittance through the parameter ε_{f1} defined in Eq. (20b). Because an anharmonic lens itself causes the beam profile to vary, ε_{f1} is often comparable in magnitude to ε_{fo}. The cumulative effect of ε_{f1} from many lenses is usually small, however, because of the varying sign and lack of coherence of ε_{f1}^2 from one lens to another; see Sec. IV-C. Not included in our analysis is the emittance change produced by the anharmonic self-pinch force, proportional to $(1-f_c)I_b$, between foils. In vacuum, the repulsive self-force, proportional to I_b/γ^2, alters the emittance.

IV. MULTI-FOIL TRANSPORT

A. Closely-Spaced Foils

The previous sections dealt with focusing from a single foil. A series of foils raises new issues, one of which is interactions between adjacent foils. Expansion (3) shows that foils interact electrically when they are separated by less than the pipe diameter, 2b. To evaluate these interactions, consider a foil located at z = 0 and an adjacent foil located at z = d. The foil potential for $0 \le z \le d$ can then be expressed as

$$\phi_f(r,z) = \sum_{n=1}^{\infty} J_o(\chi_n r/b)\,[A_n \cosh(\chi_n z/b) + B_n \sinh(\chi_n z/b)], \qquad (28)$$

in place of Eq. (3). Here A_n is given by Eq. (4), and B_n is given by

$$B_n = -\frac{2\,\mathrm{csch}(\chi_n d/b)}{\chi_n^2 J_1^2(\chi_n)} \int_0^b dr\; r\, J_o(\chi_o r/b)\left[\frac{1}{r}\frac{\partial}{\partial r}\, r\, E_{ro}(r,d)\right] - A_n \coth(\chi_n d/b). \qquad (29)$$

Note that the expansion coefficients A_n and B_n are determined solely by the ambient field E_{ro} on each of the two foils. A similar but more restrictive solution, involving a double summation, was given by Humphries.[10]

If the beam changes little between the two foils, the foil cell behaves as a single thin lens with $E_{ro}(r,d) \approx E_{ro}(r,0)$ The momentum increase imparted within the foil cell is then given by

$$\delta p_r(r) = -\int_0^d dz\, \frac{e}{c}\frac{\partial \phi_f}{\partial r} = \frac{2e}{c}\sum_{n=1}^{\infty} A_n\, J_1(\chi_n r/b)\, \frac{\cosh(\chi_n d/b)-1}{\sinh(\chi_n d/b)}, \qquad (30)$$

with A_n given by Eq. (7). A series of foil cells thus behaves as a series of thin lenses, each producing a deflection angle $\delta\theta_f$ that takes the same form as that for an isolated foil, except that the terms in the sums over n must be multiplied by $[\cosh(\chi_n d/b)-1]/\sinh(\chi_n d/b)$. The thin-lens (paraxial) treatment is valid in this case only if

$$f_\ell >> d, \qquad (31)$$

where f_ℓ is to be computed from definition (12) and result (30). This condition replaces the previous paraxial condition, $f_\ell >> b$, for widely spaced foils.

B. Axisymmetric Stability

An important issue in multi-foil transport is beam stability. To study axisymmetric stability, we treat the foils as ideal lenses, $\partial f_\ell/\partial r = 0$, and assume that the beam propagates force-free in vacuum ($f_c = 0$) between foils. The dependence of f_ℓ on beam radius R is, however, retained.

For thin lenses, the particle orbits are given by

$$x_{n+1} = x_n + x_n' d, \qquad (32a)$$

and

$$x_n' = x_{n-1}' - x_n/f_n. \qquad (32b)$$

Here x_n is the particle position at the nth lens, $x_n' = v_x/c$ is the particle

velocity just after the nth lens, and f_n is the focal length of the nth lens. Like equations describe motion in the y-direction.

For constant lens spacing d, we can eliminate x'_n to obtain a third-order difference equation for x_n:

$$x_{n+1} - 2(1 - d/2f_n)x_n + x_{n-1} = 0. \tag{33}$$

For constant f_n, this equation predicts unbounded growth unless

$$d < 4f_n. \tag{34}$$

Exponential growth[15] occurs at $d > 4f_n$, while linear growth occurs at $d = 4f_n$.

For foils, the focal length f_n is not constant but varies linearly with the rms beam radius R_n. This dependence appears to be stabilizing, because condition (34) is ultimately satisfied as R_n becomes large. More careful analysis reveals, however, that the dependence on R_n is destabilizing until R_n becomes very large. To show this, we replace difference equation (33) with an equivalent, fourth-order expression for R_n as derived in the appendix:

$$\begin{aligned}&(1-d/2f_n)R_{n+2}^2 \\ &+ [1-4(1-d/2f_{n+1})(1-d/2f_n)][(1-d/2f_{n+1})R_{n+1}^2 - (1-d/2f_n)R_n^2] \\ &- (1-d/2f_{n+1})R_{n-1}^2 = 0.\end{aligned} \tag{35}$$

Stability requirement (34) for constant f_n can be confirmed from this expression using solutions of the form $R_n = R_o \exp(i\omega n)$ and $R_n = nR_o$.

For $f_n \propto R_n$, Eq. (35) is nonlinear and difficult to analyze. We therefore consider a small perturbation about an equilibrium solution of constant radius R_o:

$$R_n = R_o [1 + \delta \exp(i\omega n)], \tag{36}$$

with $\delta \ll 1$. Inserting this form into Eq. (35) produces to order δ,

$$2(1-k)\exp[i\omega(n+2)] + k\exp(i\omega n)$$

$$+ (2-k)[1 - 4(1-k)^2]\{\exp[i\omega(n+1)] - \exp(i\omega n)\}$$

$$- 2(1-k)\exp[i\omega(n-1)] - k\exp[i\omega(n+1)] = 0, \qquad (37a)$$

where $k = d/2f_o$ is a geometrical factor and $f_o = f_n(R_o)$ is the nominal focal length.

Equation (37a) can be reduced to

$$\cos^2(\omega/2) = (1-k)(1-k/2), \qquad (37b)$$

which indicates that stable solutions (real ω) are possible only if $k \leq 1$. One can similarly show that solutions of the form $R_n = R_o\,[1 + (-)^n n\delta]$ are unstable for $k = 1$. We thus conclude that stability is possible in the linearized regime only if

$$k = d/2f_o < 1. \qquad (38)$$

This condition, which applies when $f_n \propto R_n$, is twice as restrictive as condition (34) for constant f_n.

If condition (38) is not satisfied at injection, R_n and f_n grow until the condition is satisfied. This suggests that unstable solutions would saturate if the beam were to expand slowly from foil to foil. To test whether condition (38) is actually necessary, we solved difference equation (35) numerically, using a 10% variation in R_n. Saturation occurred, if at all, only after the beam expanded to a radius much greater than R_o. We therefore conclude that multi-foil transport is in general stable only if condition (38) is satisfied at beam injection.

There are several caveats to the stability analysis. First, the underlying assumption of paraxial foil focusing is often poorly satisfied when stability condition (38) is met only marginally; preliminary numerical simulations indicate, however, that this criterion remains roughly intact even when the paraxial approximation fails. Second, the analysis neglects emittance growth from anharmonic foil focusing and scattering. Emittance

growth proportional to radius R_n ultimately causes "stable" beams to expand linearly with foil number n; to minimize n, the foil spacing d should be maximized, subject to stability condition (38). Third, the analysis assumes constant beam energy γ (and foil spacing d). If γ were to double over ten or fewer foils, beam stability and e ittance growth become much less troublesome; practical limits on average accelerating gradients make this requirement difficult to achieve, however, for high-current beams. And fourth, the analysis ignores self forces, plasma forces, and current loss to the pipe. In practice, instability often manifests itself not as total disruption but as gradual loss of the beam to the pipe walls.

C. Matching

Previous investigators[5,10] chose foil spacing based on a matching criterion in which the beam propagates unchanged from one foil cell to the next. Here we derive a matching criterion and determine if it is compatible with stability condition (38).

For a matched beam, the minimum radius, R_{min}, occurs at the mid-point of each foil cell, while the maximum radius, R_{max}, occurs at the ends. The beam expansion rate, $R' = dR/dz$, is thus anti-symmetric about the cell mid-point and about each foil. Each foil must therefore change R' to $-R'$:

$$\delta\theta_f = - R_{max}/f_\ell = - 2R'(d), \tag{39}$$

where $R'(d)$ is the expansion rate as the beam approaches a foil.

The expansion rate R' depends on the forces acting inside the foil cell. Let us consider the simple example of emittance-dominated, free expansion in vacuum ($f_c = 0$). For constant γ, the envelope equation[12] dictates that the beam expands past the cell mid-point, $z = d/2$, as

$$R^2(z) = R_{min}^2 + \left(\frac{\varepsilon}{\gamma R_{min}}\right)^2 (z - d/2)^2. \tag{40}$$

Differentiation yields the expansion rate just prior to a foil:

$$R'(d) = \left(\frac{\varepsilon}{\gamma R_{min}}\right)^2 \frac{d}{2R_{max}}. \tag{41}$$

Combining this with focusing requirement (39) and Eq. (40) produces

$$f_\ell d = \left(\frac{\gamma R_{max} R_{min}}{\varepsilon}\right)^2$$

$$\doteq \frac{\gamma^2 R_{min}^4}{\varepsilon^2} + \frac{d^2}{4}. \qquad (42)$$

Solving for the foil spacing d yields the matching requirement

$$d = 2f_\ell \left\{1 + \left[1 - \left(\frac{\gamma R_{min}^2}{\varepsilon f_\ell}\right)^2\right]^{1/2}\right\} > 2f_\ell. \qquad (43)$$

Matching requirement (43) violates stability condition (38), indicating that stable, matched propagation is not possible with foils. That is, beam stability demands closely spaced foils that overpinch the beam and cause it to vary from cell to cell. Fluctuations in beam radius need not disrupt the beam, but they do make controlling it more difficult and may accelerate emittance growth. These fluctuations also reduce contributions from the emittance change ε_{f1} by destroying beam coherence from cell to cell. Note that stable, matched propagation is possible for thin lenses of constant focal length, according to stability criterion (34).

V. OTHER CONSIDERATIONS

A. Foil Scattering

Beam electrons scatter as they pass through a foil. Although energy loss from inelastic scattering is usually negligible for the beam, it heats and may melt the foil. Foil durability is determined by the thermal properties and energy loss function of the foil.

Elastic scattering is often a greater concern and generates an angular spread in the beam of characteristic width $\delta\theta_s \propto Z\sqrt{t_f}/\gamma$, where t_f is the foil thickness and Z is the atomic number of the foil material.[16] This angular spread increases the emittance squared by an amount $\varepsilon_s^2 = (\delta\theta_s \gamma R)^2$, independent of beam current and energy. Unless the foil is a highly transparent mesh,[17] ε_s typically exceeds the increase ε_{fo} from anharmonic

focusing at beam currents below 17 kA. Note that the total emittance increase, $\varepsilon_{fo}^2 + \varepsilon_s^2$, is independent of beam energy γ; an energy ramp does not, therefore, directly alter the emittance envelope, $\varepsilon(\zeta)$.

B. Focusing by Apertures

An apparent means of avoiding or reducing collisional effects is to use conducting apertures. Apertures short $\underset{\sim}{E}_\perp$ much like foils, but they are ineffective at focusing. To show this, we use Gauss's law to express the radial impulse delivered by an isolated foil or aperture as

$$\delta p_r(r) = -\frac{e}{c}\int_{-\infty}^{\infty} dz\, E_{rf}(r,z) = -\frac{4\pi e}{rc}\int_0^r dr'\, r'\, \sigma_f(r'), \tag{44}$$

where σ_f is the surface charge density on the foil or aperture. In deriving Eq. (44) we have used the fact that the axial foil field $E_{zf} = 0$ at $z = \pm\infty$. A net impulse δp_r is thus delivered only to beam electrons that encounter enclosed surface charge. For beam electrons passing through a hole, the enclosed surface charge is zero. Hence, apertures focus only that portion of the beam <u>not</u> passing through the hole.[18] Thin apertures might, however, be useful in that they can focus the expanding beam wings while leaving the cold laminar core of the beam unperturbed.

C. Foil Focusing in a Plasma

In the preceding analysis, we allowed for a constant, self-similar charge-neutralization fraction, $f_c < 1$. This neutralization reduces the focusing action of the foil, and additionally keeps the beam pinched between foils. An important example is the ion-focused regime (IFR) in which the beam ionizes a low-pressure gas and then electrostatically expels the plasma electrons, leaving the heavy ions to pinch and guide the beam.[14] The simplicity and utility[2] of IFR transport warrants further discussion, particularly at the transition from vacuum to gas where foils are commonly employed.

Near the foil, the plasma electrons are not ejected radially because the foil shorts the transverse electric fields. However, the axial foil field E_{zf} is strong in this region and removes the plasma electrons longitudinally, either by pulling them into the foil or pushing them into

regions where they are expelled radially. In either case, only the ions remain, and hence the assumption of uniform f_c over a foil focal length is justified.

Foils are commonly used to separate regions of different gas pressure and, consequently, different neutralization fraction f_c. Because a perfectly conducting foil disrupts electromagnetic communication, the fields and impulse can be computed independently on each side of the foil. In the thin-lens limit, the total impulse and focusing effect are given by averaging f_c on the two sides. For example, at a transition from vacuum to gas, the foil focal length f_ℓ and emittance increase ε_{fo} can be computed as before, using f_c set to half its value in the gas region. The analysis of Sec. IV-A for closely spaced foils should, however, be applied without modification. Conservation of beam and field energy dictates that a change in f_c across a foil alters the axial beam momentum and energy by an amount proportional to the change.

D. Non-Axisymmetric Effects

In the previous analysis, the currents and charges induced in the pipe walls were axisymmetric and had no effect on the beam. Off-axis beams, however, induce non-axisymmetric wall currents and charges that deflect the beam. The wall return currents magnetically repel and center the beam, while the wall charges electrostatically attract the beam. Because foils neutralize the electrostatic fields, they provide a centering impulse, as well as a focusing impulse, to the beam.[5,19]

For off-axis beams, the foil potential can be expanded in terms of trignometric, exponential, and Bessel functions. The centering impulse can then be calculated using the technique given earlier for the focusing impulse. For small beam offsets, $y_b \ll b$, a simpler estimate is possible. In this case, an average foil centering force $\sim e(1-f_c)I_b y_b/b^2 c$ persists over a distance $\sim 2b$, producing[5] a centering impulse $\delta p_y \simeq 2e(1-f_c)I_b y_b/b$. Using analysis analogous to Eqs. (32)-(34), one can show that the impulse is stabilizing only for foil spacings

$$d < 4y_b p_z/\delta p_y \simeq 2bI_A/(1-f_c)I_b. \tag{45}$$

This criterion for non-axisymmetric stability is generally well satisfied

when the axisymmetric criterion (38) is satisfied and $b > 2R$.

The foil centering impulse has been claimed[5,6] to help stabilize the beam. This prediction, like condition (45), is based on a rigid-rod treatment of the beam. However, the finite transverse electromagnetic propagation time ($\sim 2b/c$) of the wall forces can cause the foil centering impulse to become out of phase with high-frequency oscillations of the beam centroid. The impulse then causes the oscillations to grow from one foil to the next, or even with distance ζ into the beam pulse. Hence, although closely spaced foils damp low-frequency transverse oscillations, they may produce instability at high frequencies.

A related concern is the beam breakup instability (BBU) which develops as transverse beam motion induces and couples to electromagnetic waves within the foil cells.[3,20,21] Adding foils increases the number of foil cavities and likely enhances BBU growth. Colombant and Lau[22] have recently concluded that BBU could explain the poor transport observed at high current in the multi-foil experiments of Meger.[9] Poor transport is also predicted, however, by the axisymmetric analysis.

Higher-order azimuthal magnetic instabilities may develop as the foils partially neutralize the electrostatic fields. Humphries and Ekdahl[17] concluded from foil experiments in vacuum that localized magnetic pinching causes beam filamentation. This azimuthal bunching saturates by raising the transverse beam pressure and emittance. Emittance growth was particularly pronounced for initially hollow beams.

VI. CONCLUSION

The theoretical analysis presented here supports earlier work[5,10] indicating the utility of foil focusing of electron beams, but it also indicates potential pitfalls and limitations. Problems arise because foil focusing depends on the beam parameters and because it is anharmonic. For example, the dependence of the foil focal length on the beam current, radius, and energy not only makes foil focusing difficult to control, as different beam segments respond differently, but it also leads to the surprising conclusion that matched, stable propagation is not possible. Instead, the beam radius oscillates in an unpredictable although mild manner as the beam propagates from foil to foil. These oscillations

aggravate emittance degradation from anharmonic foil focusing and scattering. For beam currents comparable to the Alfven current, emittance degradation from anharmonic focusing is likely to become excessive after ten or fewer foils. In general, we find that multi-foil transport, like other techniques, works best for beam currents that are small compared with the Alfven current.

ACKNOWLEDGEMENT

We thank Prof. Stan Humphries for discussing his calculations of foil focusing and transport with us, Dr. Robert Meger for sharing his experimental results with us prior to publication, and Mr. Paul Boris for aiding in the numerical evaluations of the foil focal length. This work was supported by the Defense Advanced Research Projects Agency, ARPA Order No. 4395, Amendment 86, and monitored by the Naval Surface Warfare Center.

REFERENCES

1. See, for example, J. D. Lawson, The Physics of Charged-Particle Beams, 2nd ed. (Clarendon Press, Oxford, 1988) Ch. 4.

2. D. S. Prono et al., IEEE Trans. Nucl. Sci. NS-32, 3144 (1985).

3. V. K. Neil, L. S. Hall and R. K. Cooper, Part. Accel. 9, 213 (1979).

4. W. M. Fawley et al., "Time-Dependent Degradation of an Ion-Focussed ATA Beam," Proceedings of the 1989 Particle Accelerator Conference, Chicago, Illinois, March 20-23, 1989.

5. R. J. Adler, Part. Accel. 12, 39 (1982).

6. S. Humphries, Jr. and C. Ekdahl, J. Appl. Phys. 63, 583 (1987).

7. R. J. Adler, B. Sabol and G. F. Kiuttu, IEEE Trans. Nucl. Sci. NS-30, 3198 (1983).

8. S. Humphries, Jr. and C. Ekdahl, "Experiments on Intense Electron Beam Transport in Mesh Focusing Arrays," Proceedings of 1989 Particle Accelerator Conference, Chicago, Illinois, March 20-23, 1989.

9. R. L. _ .r, private communication.

10. S. Humphries, Jr., Part. Accel. 13, 247 (1983).

11. Other authors (see refs. 5, 10) consider foil focusing to be a magnetostatic rathe than electrostatic effect, based on the concept that the foil shorts the self-electric field of the beam, leaving the self-magnetic field to pinch and focus the beam.

12. E. P. Lee and R. K. Cooper, Part Accel. 7, 83 (1976).

13. E. P. Lee, Phys. Fluids 19, 60 (1976).

14. H. L. Buchanan, Phys. Fluids 30, 221 (1987).

15. S. Humphries, Jr., Principles of Charged Particle Acceleration, (Wiley, New York City, 1986) pp. 179-182.

16. J. D. Jackson, Classical Electrodynamics (Wiley, New York City, 1962) Ch. 13.

17. S. Humphries, Jr. and C. Ekdahl, Part. Accel. 22, 1 (1988).

18. W. M. Fawley, private communication.

19. S. Humphries, C. Ekdahl and D. M. Woods, Appl. Phys. Lett. 54, 2195 (1989)

20. W. K. H. Panofsky and M. Bander, Rev. Sci. Instr. 39, 206 (1968).

21. Y. Y. Lau, Phys. Rev. Lett. 63, 1141 (1989).

22. D. Colombant and Y. Y. Lau, "BBU Estimates in Super-IBEX Foil Propagation Experiments," unpublished (1990).

APPENDIX

The transport properties of a series of thin lenses at fixed spacing d are described by Eq. (33). Here we derive an equivalent expression for ideal lenses in terms of the rms beam radius, R_n. The latter expression is useful when the focal length f_n varies with R_n.

Because R_n involves an average of x_n^2 plus y_n^2, where (x_n,y_n) is a particle position, we begin by squaring Eq. (32a) for x_{n+1} to obtain

$$x_{n+1}^2 = x_n^2 + 2x_n x_n' d + (x_n' d)^2. \tag{A1}$$

We next multiply Eq. (32a) for x_{n+1} times Eq. (32b) for x_{n+1}':

$$x_{n+1}x_{n+1}' = x_n x_n' + (x_n')^2 d - \frac{x_{n+1}(x_n + x_n' d)}{f_{n+1}}$$

$$= x_n x_n' + (x_n')^2 d - \frac{(x_n + x_n' d)x_n + x_{n+1}(x_{n+1}' + x_{n+1}/f_{n+1})d}{f_{n+1}}$$

$$= \left(1 - \frac{d}{f_{n+1}}\right) x_n x_n' - \frac{d}{f_{n+1}} x_{n+1}x_{n+1}' - \frac{x_n^2}{f_{n+1}}$$

$$- \left(\frac{x_{n+1}}{f_{n+1}}\right)^2 d + (x_n')^2 d. \tag{A2}$$

Here we have used Eqs. (32a) and (32b) to eliminate, in selected places, x_{n+1} and x_n'. Eliminating $x_n'^2$ from Eqs. (A1) and (A2) produces

$$(x_{n+1}x_{n+1}' + x_n x_n')d = \left(1 - \frac{d}{f_{n+1}}\right)x_{n+1}^2 - x_n^2. \tag{A3}$$

We now square Eq. (33), written in the form $x_{n-1} = 2(1-d/2f_n)x_n - x_{n+1}$:

$$x_{n-1}^2 = x_{n+1}^2 + 4\left(1 - \frac{d}{2f_n}\right)^2 x_n^2 - 4\left(1 - \frac{d}{2f_n}\right) x_n x_{n+1}$$

$$= x_{n+1}^2 + 4\left(1 - \frac{d}{2f_n}\right)^2 x_n^2 - 4\left(1 - \frac{d}{2f_n}\right) x_n(x_n + x_n' d), \tag{A4}$$

where we have again used Eq. (32a) to eliminate x_{n+1} from the last term. After rearrangement, this equation reduces to

$$x_n x'_n = \frac{x_{n+1}^2 - x_{n-1}^2}{4(1 - d/2f_n)d} - \frac{x_n^2}{2f_n}. \quad \text{(A5)}$$

Result (A5) can be used to eliminate $x_{n+1}x'_{n+1}$ and $x_n x'_n$ from Eq. (A3), producing

$$(1-d/2f_n)x_{n+2}^2$$

$$+ [1-4(1-d/2f_{n+1})(1-d/2f_n)][(1-d/2f_{n+1})x_{n+1}^2 - (1-d/2f_n)x_n^2]$$

$$- (1-d/2f_{n+1})x_{n-1}^2 = 0. \quad \text{(A6)}$$

A similar expression applies to y_n. If we sum and average these expressions, and invoke the perfect-lens assumption that f_n is independent of the particle positions (x_n, y_n), we obtain Eq. (35):

$$(1-d/2f_n)R_{n+2}^2$$

$$+ [1-4(1-d/2f_{n+1})(1-d/2f_n)][(1-d/2f_{n+1})R_{n+1}^2 - (1-d/2f_n)R_n^2]$$

$$- (1-d/2f_{n+1})R_{n-1}^2 = 0, \quad \text{(A7)}$$

where R_n^2 is the average of $x_n^2 + y_n^2$.

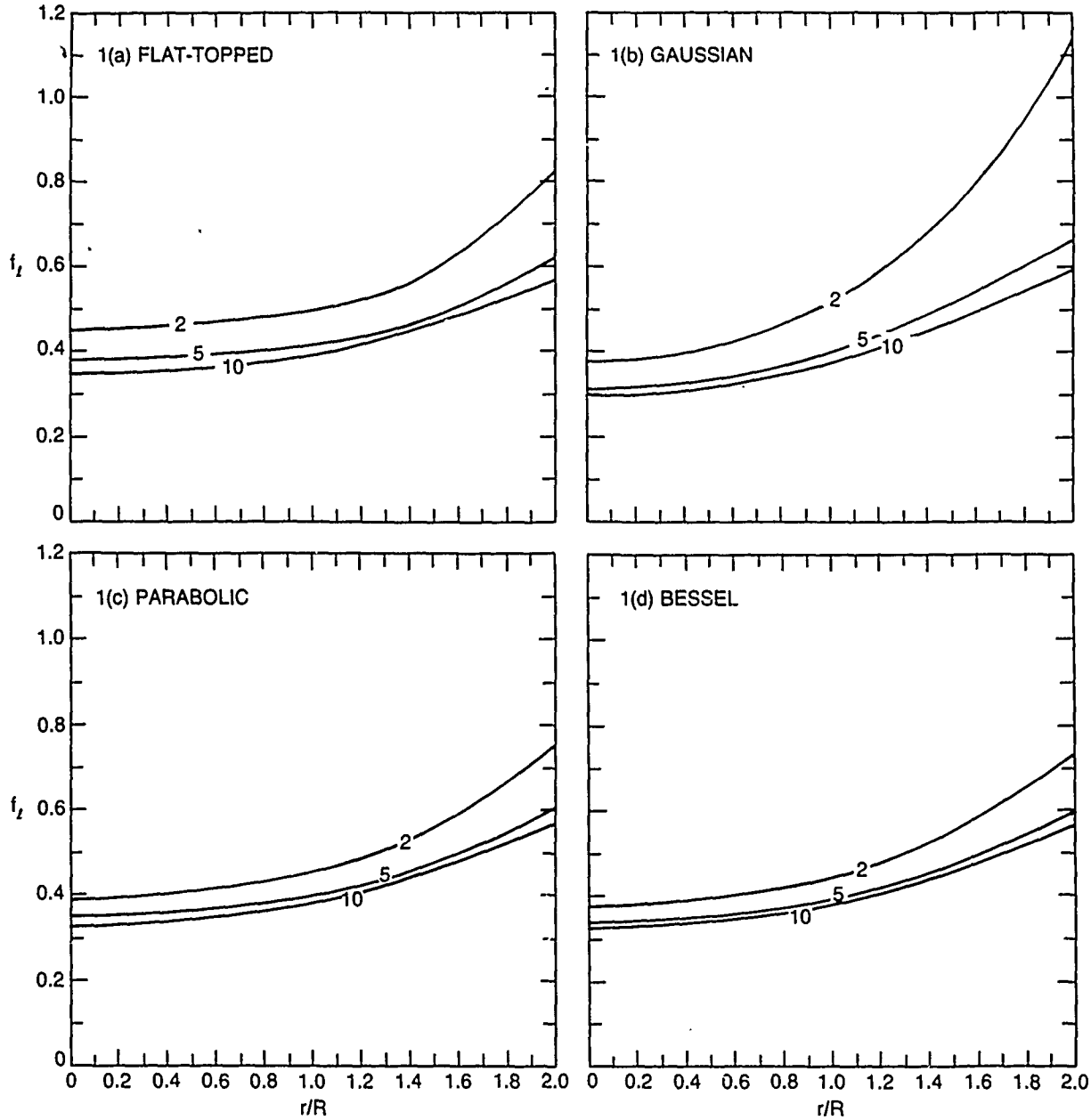

Fig. 1 The foil focal length f_ℓ expressed in units of $RI_A/(1-f_c)I_b$. No beam electrons exist outside $r/R = \sqrt{2}$ for the flat-topped profile (1a), outside $r/R = \sqrt{3}$ for the parabolic profile (1c), and outside $r/R \simeq 1.8$ for the Bessel profile (1d). The Gaussian profile (1b) extends to the wall.

Distribution List*

Naval Research Laboratory
4555 Overlook Avenue, S.W.
Attn: CAPT J. J. Donegan, Jr. - Code 1000
Dr. M. Lampe - Code 4792 (20 copies)
Dr. T. Coffey - Code 1001
Head, Office of Management & Admin - Code 1005
Deputy Head, Office of Management & Admin - Code 1005.1
Directives Staff, Office of Management & Admin - Code 1005.6
Director of Technical Services - Code 2000
ONR - Code 0124
NRL Historian - Code 2604
Dr. W. Ellis - Code 4000
Dr. J. Boris - Code 4040
Dr. M. Picone - Code 4040
Dr. M. Rosen - Code 4650
Dr. M. Haftel - Code 4665
Dr. S. Ossakow - Code 4700 (26 copies)
Dr. A. Robson - Code 4708
Dr. M. Friedman - Code 4750
Dr. R. Meger - Code 4750
Dr. J. Antoniades - Code 4751
Dr. T. Peyser - Code 4751
Dr. D. Murphy - Code 4751
Dr. R. Pechacek - Code 4750.1
Dr. G. Cooperstein - Code 4770
Dr. A. Ali - Code 4780
Dr. D. Colombant - Code 4790
Dr. R. Fernsler - Code 4790 (25 copies)
Dr. S. Gold - Code 4790
Dr. I. Haber - Code 4790
Dr. R. F. Hubbard - Code 4790 (25 copies)
Dr. G. Joyce - Code 4790
Dr. Y. Lau - Code 4790
Dr. S. P. Slinker - Code 4790 (25 copies)
Dr. P. Sprangle - Code 4790
Dr. R. Taylor - 4790
Dr. J. Krall - Code 4790
B. Pitcher - Code 4790A
Code 4790 (20 copies)
Mr. P. Boris - SAIC (Code 4790)
Library - Code 2628 (22 copies)
D. Wilbanks - Code 2634
Code 1220

* Every name listed on distribution gets one copy except for those where extra copies are noted.

Air Force Office of Scientific Research
Physical and Geophysical Sciences
Bolling Air Force Base
Washington, DC 20332
Attn: Major Bruce Smith

Air Force Weapons Laboratory
Kirtland Air Force Base
Albuquerque, NM 87117-6008
Attn: William L. Baker (AFWL/NTYP)
Breddan B. Godfrey

U. S. Army Ballistics Research Laboratory
Aberdeen Proving Ground, Maryland 21005
Attn: Dr. Donald Eccleshall (DRXBR-BM)
Dr. Anand Prakash
Dr. Clinton Hollandsworth

Avco Everett Research Laboratory
2385 Revere Beach Pkwy
Everett, Massachusetts 02149
Attn: Dr. R. Patrick
Dr. Dennis Reilly

Ballistic Missile Def. Ad. Tech. Ctr.
P.O. Box 1500
Huntsville, Alabama 35807
Attn: Dr. M. Hawie (BMDSATC-1)

Chief of Naval Material
Office of Naval Technology
MAT-0712, Room 503
800 North Quincy Street
Arlington, VA 22217
Attn: Dr. Eli Zimet

Commander
Space and Naval Warfare Systems Command
National Center 1, Room 8E08
Washington, DC 20363-5100
Attn: RADM Robert L. Topping

Cornell University
369 Upson Hall
Ithaca, NY 14853
Attn: Prof. David Hammer

DASIAC - DETIR
Kaman Tempo
25600 Huntington Avenue, Suite 500
Alexandria, VA 22303
Attn: Mr. F. Wimenitz

Defense Advanced Research Projects Agen
1400 Wilson Blvd.
Arlington, VA 22209
Attn: Dr. H. L. Buchanan
Dr. B. Hui

Defense Nuclear Agency
Washington, DC 20305
Attn: Dr. Muhammad Owais (RAAE)

Department of Energy
Washington, DC 20545
Attn: Dr. Wilmot Hess (ER20:GTN,
High Energy and Nuclear Physics)
Mr. Gerald J. Peters (G-256)

Directed Technologies, Inc.
1500 Wilson Blvd. Suite 515
Arlington, VA 22209
Attn: Mr. Ira F. Kuhn
Dr. Nancy Chesser

C. S. Draper Laboratories
555 Technology Square
Cambridge, Massachusetts 02139
Attn: Dr. E. Olsson

General Dynamics Corporation
Pomana Division
1675 W. Mission Blvd.
P. O. Box 2507
Pomana, CA 92769-2507
Attn: Dr. Ken W. Hawko

Hy-Tech Research Corp.
P. O. Box 3422 FSS
Radford, VA 24143
Attn: Dr. Edward Yadlowsky

HQ Foreign Technology Division
Wright-Patterson AFB, OH 45433
Attn: TUTD/Dr. C. Joseph Butler

Institute for Defense Analyses
1801 N. Beauregard Street
Alexandria, VA 22311
Attn: Dr. Deborah Levin
Ms. M. Smith

Intelcom Rad Tech.
P.O. Box 81087
San Diego, California 92138
Attn: Dr. W. Selph

JAYCOR
11011 Torreyana Road
P. O. Box 85154
San Diego, CA 92138-9259
Attn: Dr. Franklin S. Felber
Dr. Seung Kai Wong

JAYCOR
39650 Libery Street, Suite 320
Freemont, CA 94538
Attn: Dr. Kendal Casey

Joint Institute for Laboratory
Astrophysics
National Bureau of Standards and
University of Colorado
Boulder, CO 80309
Attn: Dr. Arthur V. Phelps

Kaman Sciences
1500 Garden of the Gods Road
Colorado Springs, CO 80933
Attn: Dr. John P. Jackson

Kaman Sciences
P. O. Drawer QQ
Santa Barbara, CA 93102
Attn: Dr. W. Hobbs

La Jolla Institute
P. O. Box 1434
La Jolla, CA 92038
Attn: Dr. K. Brueckner

Lawrence Berkeley Laboratory
University of California
Berkeley, CA 94720
Attn: Dr. Edward P. Lee
Dr. Thomas Fessenden

Lawrence Livermore National Laboratory
University of California
Livermore, California 94550
Attn: Dr. Simon S. Yu
Dr. Frank Chambers
Dr. James W.-K. Mark, L-477
Dr. William Fawley
Dr. William Barletta
Dr. William Sharp
Dr. Daniel S. Prono
Dr. John K. Boyd
Dr. John Clark
Dr. George J. Caporaso
Dr. Donald Prosnitz
Dr. John Stevart
Dr. Y. P. Chong
Major Kenneth Dreyer
Dr. Hans Kruger
Dr. Thaddeus J. Orzechowski
Dr. Michael R. Teague
Mr. John T. Weir

Dr. James E. Leiss
13013 Chestnut Oak Drive
Gaithersburg, MD 20878

Lockheed Missiles and Space Co.
3251 Hanover St.
Bldg. 205, Dept 92-20
Palo Alto, CA 94304
Attn: Dr. John Siambis

Los Alamos National Laboratory
P.O. Box 1663
Los Alamos, NM 87545
Attn: Dr. L. Thode
Dr. H. Dogliani, MS-5000
Mr. R. Carlson, MS-P940
Dr. Carl Ekdahl, MS-D410
Dr. Joseph Mack
Dr. Melvin I. Buchwald
Dr. David C. Moir

Maxwell Laboratories Inc.
8888 Balboa Avenue
San Diego, CA 92123
Attn: Dr. Ken Whitham

McDonnell Douglas Research Laboratories
Dept. 223, Bldg. 33, Level 45
Box 516
St. Louis, MO 63166
Attn: Dr. Carl Leader
Dr. Frank Bieniosek
Dr. John Honig

Mission Research Corporation
1720 Randolph Road, S.E.
Albuquerque, NM 87106
Attn: Dr. Thomas Hughes
Dr. Lawrence Wright
Dr. Kenneth Struve
Dr. Michael Mostrom
Dr. Dale Welch

Mission Research Corporation
P. O. Drawer 719
Santa Barbara, California 93102
Attn: Dr. C. Longmire
Dr. N. Carron

National Inst. of Standards & Tech.
Gaithersburg, Maryland 20760
Attn: Dr. Mark Wilson

Naval Postgraduate School
Physics Department (Code 61)
Monterey, CA 93940
Attn: Prof. John R. Neighbours
Prof. Fred Buskirk
Prof. Kai Woehler
Prof. Xavier Maruyama

Naval Surface Warfare Center
White Oak Laboratory
Code R-41
Silver Spring, Maryland 20903-5000
Attn: Mr. W. M. Hinckley
Dr. M. H. Cha
Dr. H. S. Uhm
Dr. R. Fiorito
Dr. K. T. Nguyen
Dr. R. Stark
Dr. H. C. Chen
Dr. D. Rule
Dr. Matt Brown
Mrs. Carolyn Fisher (G42)
Dr. Eugene E. Nolting (H23)

Office of Naval Research
800 North Quincy Street
Arlington, VA 22217
Attn: Dr. C. W. Roberson
Dr. F. Saalfeld

Office of Naval Research (2 copies)
Department of the Navy
Code 01231C
Arlington, VA 22217

Office of Under Secretary of Defense
Research and Engineering
Room 3E1034
The Pentagon
Washington, DC 20301
Attn: Dr. John MacCallum

Physics International, Inc.
2700 Merced Street
San Leandro, CA. 94577
Attn: Dr. E. Goldman
Dr. James Benford
Dr. George B. Frazier
Mr. Ralph Genuario

Princeton University
Plasma Physics Laboratory
Princeton, NJ 08540
Attn: Dr. Francis Perkins, Jr.

Pulse Sciences, Inc.
600 McCormack Street
San Leandro, CA 94577
Attn: Dr. Sidney Putnam

Pulse Sciences, Inc.
2001 Wilshire Boulevard
Suite 600
Santa Monica, CA 90403
Attn: Dr. John R. Bayless
Dr. R. Adler

The Rand Corporation
2100 M Street, NW
Washington, DC 20037
Attn: Dr. Nikita Wells
Mr. Simon Kassel

Sandia National Laboratory
Albuquerque, NM 87115
Attn: Dr. David Hasti/1272
Dr. Collins Clark
Dr. John Freeman/1241
Dr. Charles Frost
Dr. George Kamin/1274
Dr. Gordon T. Leifeste
Dr. Gerald N. Hays
Dr. Michael G. Mazarakis/1272
Dr. John Wagner/1241
Dr. Ron Lipinski/1274
Dr. James Poukey
Dr. Milton J. Clauser/1261
Dr. Kenneth R. Prestwich/1240
Dr. Kevin O'Brien
Dr. Isaac R. Shokair
Dr. J. Pace VanDevender/1200

Science Applications Intl. Corp.
5150 El Camino Road
Los Altos, CA 94022
Attn: Dr. R. R. Johnston
Dr. Leon Feinstein
Dr. Douglas Keeley
Dr. E. Roland Parkinson

Science Applications Intl. Corp.
1710 Goodridge Drive
McLean, VA 22102
Attn: Mr. W. Chadsey
Dr. A Drobot
Dr. K. Papadopoulos
Dr. William W. Rienstra
Dr. Alan J. Toepfer
Dr. Alfred Mondelli
Dr. D. Chernin
Dr. R. Tsang

Science Research Laboratory, Inc.
1600 Wilson Boulevard
Suite 1200
Arlington, VA 22209
Attn: Dr. Joseph Mangano
Dr. Daniel Birx

Commander
Space & Naval Warfare Systems Command
PMW-145
Washington, DC 20363-5100
Attn: CAPT J. D. Fontana
LT Fritchie

SRI International
PS0-15
Molecular Physics Laboratory
333 Ravenswood Avenue
Menlo Park, CA 94025
Attn: Dr. Donald Eckstrom
Dr. Kenneth R. Stalder

Strategic Defense Initiative Org.
SDIO/T/DE0
The Pentagon
Washington, DC 20009-7100
Attn: Lt Col R. L. Gullickson
Dr. D. Duston

Titan/Spectron, Inc.
P. O. Box 4399
Albuquerque, NM 87196
Attn: Dr. R. Bruce Miller
Dr. John Smith

Titan Systems, Inc.
2685 Marine Way
Suite 1408
Mountain View, CA 94043
Attn: Dr. Kenneth W. Billman

Titan Systems, Inc.
9191 Towne Centre Dr.-Suite 500
San Diego, CA 92122
Attn: Dr. R. M. Dove

University of California
Physics Department
Irvine, CA 92664
Attn: Dr. Gregory Benford
Dr. Norman Rostoker

University of California
San Diego, CA 92110
Attn: Dr. Marshall N. Rosenbluth

UCLA
Physics Department
Los Angeles, CA 90024
Attn: Dr. F. Chen
Dr. C. Joshi
Dr. J. Dawson
Dr. N. Luhmann

University of Maryland
Physics Department
College Park, MD 20742
Attn: Dr. Y. C. Lee
Dr. C. Grebogi
Dr. W. Destler
Dr. C. Striffler

University of Michigan
Dept. of Nuclear Engineering
Ann Arbor, MI 48109
Attn: Prof. Terry Kammash
Prof. R. Gilgenbach

Director of Research
U.S. Naval Academy
Annapolis, MD 21402 (2 copies)

Do NOT make labels for
Records-----(01 cy)

Naval Research Laboratory
Washington, DC 20375-5000
Code 4830
Timothy Calderwood

Naval Research Laboratory
Washington, DC 20375-5000
Code 1220